Chapter 2

Thermomechanics of Solid Oxide Fuel Cell Electrode Microstructures Using Finite Element Methods: Progressive Interface Degradation under Thermal Cycling

Sushrut Vaidya and Jeong ho Kim

Abstract

The electrochemical performance of solid oxide fuel cell (SOFC) is significantly influenced by three-phase boundary (TPB) zones in the microstructure. TPB zones are locations where all three phases comprising the microstructure such as the two solid phases and the pore phase are present. Electrochemical reactions such as oxygen reduction occur near TPBs, and TPB density is believed to affect the polarization resistance of the cathode. In this regard, the effect of interface degradation under repeated thermal loading on the mechanical integrity and electrochemical performance of solid oxide fuel cell (SOFC) electrodes is studied through finite element simulations. Image-based 3-D models are used in this study, with additional interface zones at the boundaries between dissimilar solid phases. These interface zones are composed of 3-D cohesive elements of small thickness. The effect of interface degradation on mechanical integrity is studied by subjecting 50:50 LSM:YSZ wt.% cathode models to increasing levels of thermal load from room temperature (20°C) up to operating temperature (820°C). Energy quantities (e.g., strain energy and damage dissipation) for cathode models with and without cohesive interface zones are obtained through finite element analysis (FEA). These quantities are compared using energy balance concepts from fracture mechanics to gain insight into the effects of interface degradation on mechanical integrity.

Keywords: solid oxide fuel cells, cathode, thermal cycling, probability of failure, finite element analysis

1. Introduction

Solid oxide fuel cells (SOFCs) are capable of converting chemical energy into electrical energy with high efficiency and low emissions [1]. Anode, cathode, electrolyte, and interconnect wires are the basic components of SOFCs [1]. SOFCs have been investigated for such configurations [2, 3], materials [4–8], component

microstructures [9–12], electrochemical performance [11–14], and thermal stresses [14–17]. A variety of approaches have been chosen to investigate problems related to SOFCs: analytical [3], experimental [4–12], and computational [2, 13–17]. Research has shown that electrochemical performance of SOFCs is affected by component microstructure [11, 12]. In contrast, few studies have investigated the effects of microstructure on mechanical performance [16]. Mechanical durability of the SOFC is a significant factor for performance. It is important to understand the effect of microstructure on durability and probability of failure under thermal loads.

We perform finite element analysis (FEA) of thermal stresses induced in reconstructed SOFC cathode microstructures under thermal cycling. 3-D finite element (FE) models of SOFC cathode microstructures are generated from a stack of 2-D microstructure images. Anode (50:50 wt.% NiO:YSZ) and cathode (50:50 wt.% LSM:YSZ) microstructures have previously been analyzed and validated for thermal stress using finite elements by the authors [17]. This study extends the work by investigating the effect of interface degradation under repeated thermal loading on the mechanical integrity and electrochemical performance of SOFC electrodes through finite element simulations. The effect of interface degradation on mechanical integrity is studied by subjecting 50:50 LSM:YSZ wt.% cathode models to increasing levels of thermal load from room temperature (20°C) up to operating temperatures (820°C). Energy quantities (e.g., strain energy and damage dissipation) for cathode models with and without cohesive interface zones are obtained through FEA. These quantities are compared using energy balance concepts from fracture mechanics to gain insight into the effects of interface degradation on mechanical integrity. The electrochemical performance of SOFCs is significantly influenced by three-phase boundary (TPB) zones in the microstructure. TPB zones are locations where all three phases comprising the microstructure—the two solid phases and the pore phase—are present. Electrochemical reactions such as oxygen reduction occur near TPBs, and TPB density is believed to affect the polarization resistance of the cathode [5, 18]. In this study, we hypothesize that degradation of weak interfaces under thermal cycling has an adverse effect on TPB zones in the microstructure of the SOFC, leading to a reduction in electrochemical performance over time. Interface degradation under thermal cycling is implemented in the FE electrode models through a simplified scheme. The scheme consists of five successive monotonic, steady-state heating operations from room temperature (20°C) up to operating temperature (820°C), combined with interface strength and fracture energy degradation in each heating operation. Each thermal loading operation represents the heating phase of a normalized thermal cycle, where one normalized cycle represents 1000 actual thermal cycles. SOFCs have been known to perform with great reliability, showing no reduction in performance, for more than 2 years at a stretch [1]. Thus, it may be reasonable to assume that one normalized heating cycle in this study represents 1000 actual thermal cycles in the operating life of the cell. The interface degradation scheme is explained in detail later.

2. Image-based finite element microstructure models

3-D FE microstructure models were reconstructed from 41 2-D cross-sectional images of cathode microstructures [9, 10], using focused ion beam-scanning electron microscopy (FIB-SEM). Examples of the 2-D images are shown in **Figure 1**. These images are of the real cathode microstructures having 50:50 LSM:YSZ composition.

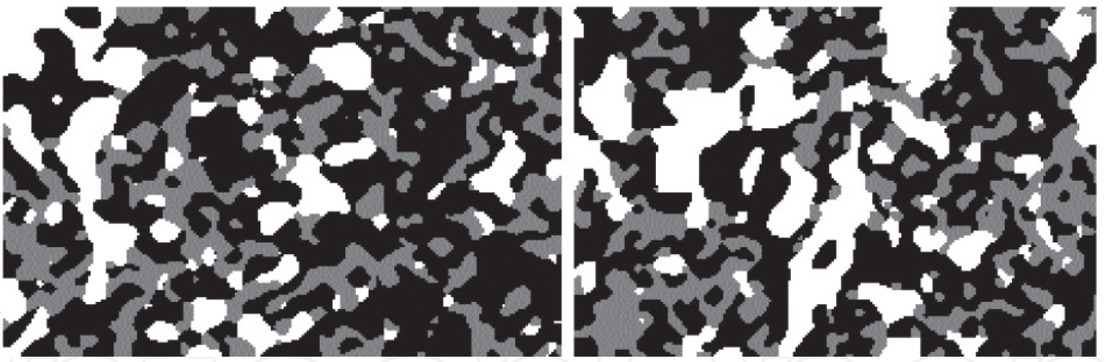

Figure 1.
2-D SEM images of typical cross-sections of 50:50 wt.% LSM:YSZ cathode [9, 10].

In the SEM cathode images, white (pixel value = 255) represents LSM, gray (pixel value = 127) represents YSZ, and black (pixel value = 0) represents the pores. The original cathode image has 217 pixels (width) × 147 pixels (height). The x-y (in-plane) spatial resolution between pixels is 40.8 nm and the z-spacing between images is 53.3 nm. The cathode images are thus of size 8.85 μm (width) × 6.00 μm (height). Finite element modeling was carried out using the commercial FE software Abaqus [19] for which MATLAB® [20] was to create input files. The 3-D FE model was reconstructed from the 2-D images using 3-D finite elements (eight-node brick elements). In order to increase computational efficiency for 3-D analysis using finite element method, we reduced the full model to a representative model in which we sacrifice some details of phase geometry but microstructural skeleton that is crucial to stress analysis remains almost unchanged. To provide validation data for this present approach, we used 2-D cathode microstructure images and calculated the three-phase boundary (TPB) density and phase surface area density for the original, full-size 50:50 wt.% LSM:YSZ cathode, as well as the reduced 50:50 cathode. The data agreed reasonably well with those reported in the literature [10, 12, 21].

The original images of the cathode were simplified by sampling pixels at regular intervals to reduce the image resolution while retaining a detailed microstructure. The simplified cathode images were 3.51 μm (width) × 3.02 μm (height) in size. The depth of the voxel was 53.3 nm. A stack of all the 2-D images was created in the z-direction by using a cell array construct to arrange the images consecutively. An initially blank "buffer" plane was then introduced between consecutive images. The gaps between consecutive images were filled by assigning one eight-node brick element to each voxel. Thus, the geometry of the cathode microstructure was reconstructed in the 3-D FE models, with a step variation in material regions between consecutive images. The volume fractions of phases in each 3-D model were calculated by counting the number of voxels corresponding to each phase (based on pixel value) and dividing by the total number of voxels in the model. Information concerning the material properties, boundary conditions, initial temperature, temperature field and required outputs was also specified in the input file.

3. Thermomechanical material properties

Finite element analyses of the LSM/YSZ (50:50 wt.%) cathode microstructure models were carried out to investigate thermal stresses due to various temperature fields. The effects of varying phase volume fractions and temperature-dependent material properties on thermal stresses and probability of failure were investigated. The FE model was subjected to fixed boundary conditions. The behavior of the

Material	Young's modulus (GPa)	Poisson's ratio	CTE (10^{-6} °C^{-1})
YSZ	205	0.30	10.40
LSM	40	0.25	11.40

Table 1.
Room temperature material properties used in FE analyses of cathode [3, 22].

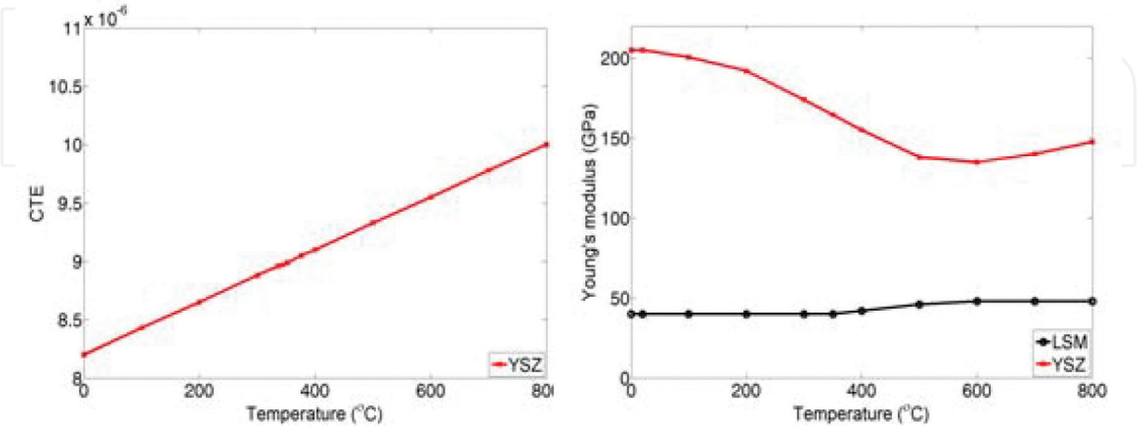

Figure 2.
Variation of CTE of YSZ with temperature [16]; variation of Young's modulus of LSM and YSZ with temperature [12].

model with increasing temperature loads was investigated by subjecting the model to eight different spatially uniform predefined temperature fields of magnitude 120, 220, 320, ..., 820°C. In each analysis, the initial temperature was specified as 20°C (room temperature), so that the model was subjected to eight different magnitudes of temperature change (ΔT = 100, 200, 300, ..., 800°C). **Table 1** lists the room temperature material properties used for YSZ and LSM [3, 22].

Figure 2 shows the variation of the CTE of YSZ with temperature [22] and the variation of Young's modulus of LSM and YSZ with temperature [4]. The CTE of LSM was assumed constant over the temperature range considered. The room temperature value of the CTE of LSM was used in the FE analyses.

4. Finite element analysis using cohesive interface model

An interface damage initiation and evolution model is implemented in the 3-D finite element (FE) SOFC electrode microstructures. The thin interface zones between dissimilar solid phases consist of 3-D cohesive elements. The 3-D cohesive elements, which are of negligible thickness compared with the neighboring solid elements, are used to simulate debonding between different solid phases at their interface. The 3-D cohesive elements are inserted between eight-node 3-D linear brick elements belonging to dissimilar solid phases, as shown in **Figure 3**. Based on the in-plane (x-y) dimensions of the solid elements in the anode (14.0 nm) and cathode (40.8 nm), the thickness of the thin interface cohesive elements is chosen as 1 nm. Interfacial (fracture) energy is used as a reference value for bond strength between LSM and YSZ (cathode). Perfect bonding is assumed between elements belonging to the same solid phase. An algorithm based on the boundary pixel identification scheme is used to identify elements lying on solid-phase boundaries.

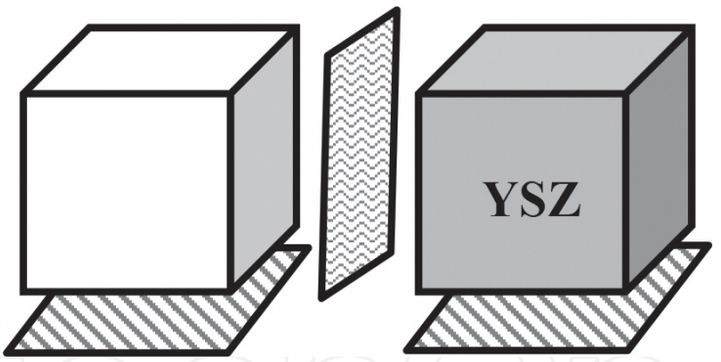

Figure 3.
Cohesive elements in the interface zone between solid elements of different phases. Vertical and horizontal cohesive elements are used.

4.1 Traction-separation behavior of cohesive elements

The behavior of the interface cohesive zone elements is described using a traction-separation relation. Such a cohesive zone model (CZM) describes local material separation behavior by relating tractions ($\boldsymbol{t}$) on the interface surfaces to material separation ($\boldsymbol{\delta}$). The CZM simulates progressive damage in the cohesive zone. The CZM is used to model imperfect bonding in highly porous electrodes of SOFCs. In three dimensions, the traction-separation model for cohesive elements consists of three deformation modes: one normal mode and two in-plane shear modes. In the normal mode, the deformation is purely in a direction perpendicular to the plane of the interface. In the two in-plane shear modes, the deformation is parallel to the plane of the interface. Thus, for 3-D cohesive elements, the traction vector ($\boldsymbol{t}$) has three components: one normal component (i.e., perpendicular to the plane of the interface), t_n, and two in-plane shear components, t_s and t_t, parallel to the plane of the interface. The separation vector ($\boldsymbol{\delta}$) has three corresponding components, δ_n, δ_s, and δ_t. The nominal strain components can then be written as follows:

$$\varepsilon_n = \frac{\delta_n}{T_0};\ \varepsilon_s = \frac{\delta_s}{T_0};\ \varepsilon_t = \frac{\delta_t}{T_0} \tag{1}$$

Here, T_0 is the initial thickness of the interface. If we set $T_0 = 1$, the nominal strain components become numerically equal to the corresponding separation components. This rescaling can be achieved by defining the interface stiffness (K_i) as follows:

$$K_i = \frac{E_i}{T_0} \tag{2}$$

E_i is the Young's modulus of the interface material and T_0 is the initial thickness of the interface. In this study, the weak interfaces between dissimilar solid phases are modeled using cohesive elements with linear elastic traction-separation behavior up to damage initiation, followed by linear stiffness degradation, to simulate damage evolution. A linear stiffness degradation model has been used by Xiao et al. [23] to study the fracture behavior of ultra-high strength concrete. Thus, the linear damage evolution model may be appropriate for describing the degradation of SOFC electrode interfaces between dissimilar solid (ceramic) phases that exhibit brittle behavior. The normal and in-plane modes of the traction-separation model used in this study are assumed to be uncoupled. The uncoupled linear elastic

constitutive behavior of the cohesive elements can be expressed as follows, in terms of tractions $\boldsymbol{t}$ and separations $\boldsymbol{\delta}$ (which are numerically equal to strains ε):

$$\boldsymbol{t} = \begin{Bmatrix} t_n \\ t_s \\ t_t \end{Bmatrix} = \begin{bmatrix} K_{nn} & 0 & 0 \\ 0 & K_{ss} & 0 \\ 0 & 0 & K_{tt} \end{bmatrix} \begin{Bmatrix} \varepsilon_n \\ \varepsilon_s \\ \varepsilon_t \end{Bmatrix} = \boldsymbol{K_i \varepsilon} \tag{3}$$

The uncoupled behavior of the cohesive elements is indicated by the fact that all off-diagonal terms are zero in the interface stiffness ($\boldsymbol{K_i}$) matrix in the constitutive traction-separation ($\boldsymbol{t}$-$\boldsymbol{\delta}$) relation given earlier. **Figure 4** is a schematic representation of the traction-separation curve for LSM/YSZ interface cohesive elements used in this study. In **Figure 4**, δ^0 is the critical separation at which damage is initiated in the cohesive element. Similarly, δ^f is the final separation at the ultimate failure of the cohesive element.

Based on the approach adopted by Nguyen et al. [24], a quadratic stress interaction equation is used to describe the damage initiation condition:

$$\left(\frac{\langle t_n \rangle}{t_n^0}\right)^2 + \left(\frac{t_s}{t_s^0}\right)^2 + \left(\frac{t_t}{t_t^0}\right)^2 = 1 \tag{4}$$

Here, t_n^0, t_s^0, and t_t^0 denote the maximum nominal stress when the deformation is either purely in a direction perpendicular to the plane of the interface or in one of the two orthogonal directions lying in the plane of the interface. The Macaulay brackets < > enclosing t_n indicate that only tensile normal stress causes damage initiation in the cohesive elements. Purely compressive normal stress causes no damage in the cohesive layer [25]. This equation is used to describe the damage initiation criterion for the interface, accounting for the interaction between the normal (tensile) and in-plane (shear) stresses. Due to lack of detailed experimental data on the strength and stiffness properties of the LSM/YSZ interfaces, the approach used by Nguyen et al. [24] is adopted for the cathode: the normal tensile strength and in-plane shear strengths of the LSM/YSZ interface are all assumed to be equal to the Weibull strength of the weaker phase (LSM), that is, 52 MPa [26, 27]. The stiffness of the LSM/YSZ interface is assumed to be characterized by the Young's modulus of

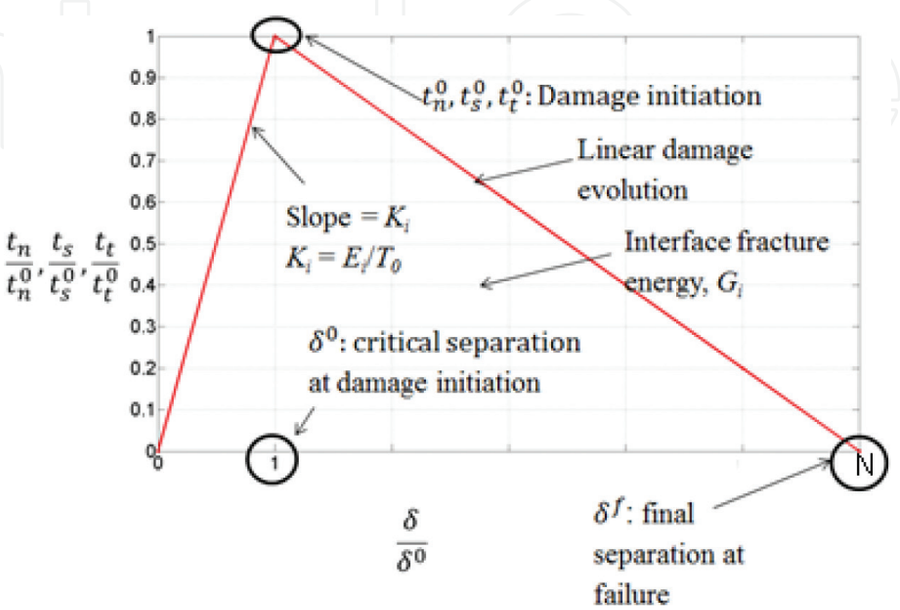

Figure 4.
Schematic diagram of traction-separation curve for an interface.

LSM (40 GPa) [4]. Stiffness degradation does not occur for the cohesive elements under pure normal compressive stress.

The definitions of damage evolution used in this study are based on the fracture energies of the LSM/YSZ interface (cathode). The fracture energy (per unit interface area) is the area under the traction-separation curve for the interface. The critical energy release rate (G_i) for the LSM/YSZ interface is taken as 7.80 J m^{-2} [11]. Based on numerical simulation results reported in the literature [11], the interface is assumed to fail in pure Mode I (normal mode) loading conditions. This leads to a mode-mix ratio ψ = 0° based on traction components. The Young's modulus and original thickness of the LSM/YSZ interface are used to calculate its normalized stiffness K_i (40 x 10^9 N mm^{-3}). The stiffness K_i and interface strength are used to calculate the critical separation δ^0 (0.0013 nm). The area under the traction-separation curve is equal to the fracture energy per unit interface area, 7.80 J m^{-2}. This is used to calculate the final separation at ultimate failure, δ^f (0.3 μm).

4.2 Interface degradation scheme

Degradation of the interface and TPB zones between dissimilar solid phases under repeated thermal cycling may be one of the major reasons for degradation of SOFC performance over time. In this study, interface degradation with thermal cycling is simulated using a simplified scheme. Only the heating phase of the thermal cycle is simulated. Steady-state conditions are assumed and transient effects are neglected. The models are subjected to five successive steady-state heating operations. Each analysis utilizes a spatially uniform temperature field to simulate steady-state heating of the model from room temperature (20°C) up to operating temperature (820°C). Progressive interface degradation is simulated by decreasing the stress at which damage begins in the cohesive interface layers in each successive analysis. The critical and final separations for the cohesive elements are assumed to remain unchanged over the five heating cycles, leading to a progressive reduction of both interface stiffness and critical energy release rate, as shown schematically in **Figure 5**.

Critical energy release rate (i.e., fracture energy per unit interface area) is a measure of the resistance of the interface material to damage [28, 29], while stiffness is indicative of the amount of damage (i.e., stiffness decreases as damage progresses). Therefore, both stiffness and fracture energy are assumed to progressively decrease with thermal cycling. Thus, this scheme implements interface degradation in a

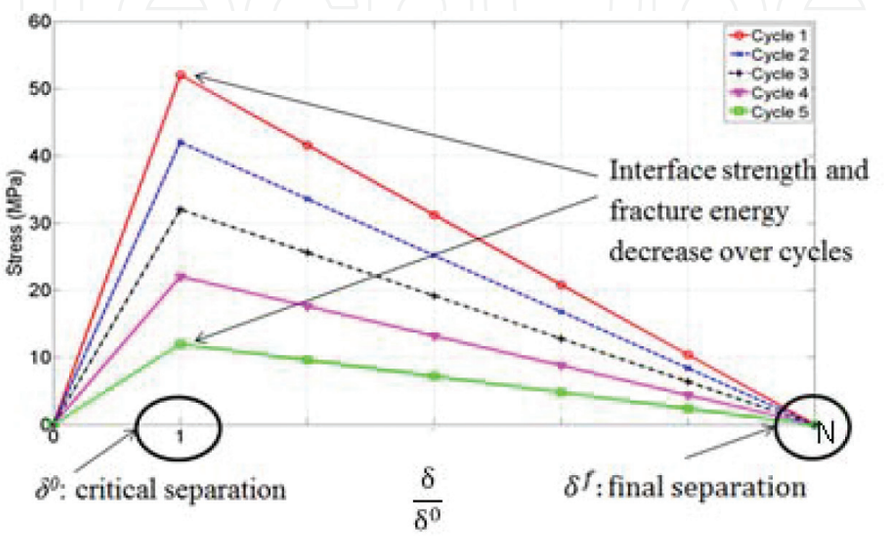

Figure 5.
Schematic diagram of interface degradation model.

simplified manner. Mechanical degradation of the interface is considered, without considering interface degradation due to electrochemical or redox processes. The earlier scheme is only a first approximation to the complex degradation processes that occur at the actual interfaces in a real SOFC electrode. Multiphysics simulations considering both mechanical and electrochemical degradation processes may be an interesting topic for future research.

4.3 Study design

Two sets of electrode microstructure models are generated. One set has perfect bonding throughout the entire model and the other has cohesive zones between dissimilar solid phases. Image-based 3-D models similar to those described in previous sections are used here, with one important difference. The models used are derived through image simplification by analyzing (2×2) pixel squares in the original images. This scheme increases the effective pixel size but preserves both the overall size of the image and the depth of the voxel, leading to a decrease in the reconstructed volume due to the use of a limited number of images. However, this scheme leads to a reasonably good approximation of the original microstructure. In the present study, a similar approach is used to simplify the model. An algorithm is devised to analyze consecutive pixel squares of $(n \times n)$ pixels in each original image. For each such square, the number of pixels belonging to each phase is counted. The phase that contributes the maximum number of pixels to the $n \times n$ pixel square is assigned as the final phase of the single pixel at that location in the simplified image. Additionally, in the present approach, preservation of the original volume of the electrode model in the simplified version is implemented by causing an increase in both effective pixel size and effective voxel depth. The volumes of the simplified models used here are 112.18 μm^3 for the anode and 670.35 μm^3 for the cathode. The cathode volume may be compared against the sampled volume of 178 μm^3 for the simplified cathode model. The values of n used in this study are as follows: for the cathode, $n = 6$, and for the anode, $n = 10$. These levels of simplification are necessary to achieve reasonable computational time for each FE analysis. A detailed validation study for this new approach based on volume fractions, phase surface area densities, and TPB densities may be an interesting topic for future research. In the present study, the plausibility of this new approach is demonstrated by showing that TPB density values obtained for cathode models lie within physically reasonable limits of experimentally determined ranges for these values.

Increasing levels of thermal load are applied through spatially uniform temperature fields of magnitude 120°C, 220°C,..., 820°C, to simulate steady-state heating from room temperature (20°C) up to operating temperature. Energy quantities (e.g., strain energy and damage dissipation) are calculated from FEA for each $\Delta T = 100°C, 200°C,..., 800°C$. The energy quantities for models with and without cohesive zones are compared to gain insight into the effect of weak interface zones between dissimilar solid phases on the mechanical integrity of the cathode. Energy concepts from fracture mechanics are used to interpret the results obtained. This procedure is performed using the cathode microstructure model, considering the original composition (50:50 wt.% LSM:YSZ). In the second part of the study, three-phase boundary (TPB) evolution under repeated, steady-state, monotonic thermal loads is studied using 50:50 wt.% electrode microstructure models. Electrode models with cohesive interface zones are subjected to five successive monotonic, steady-state, heating operations from room temperature up to operating temperature ($\Delta T = +800°C$) using a spatially uniform temperature field. During each successive analysis, the strength of the cohesive interface between dissimilar solid phases is decreased to simulate the effect of interface degradation under thermal

cycling. Progressive interface degradation under thermal cycling is implemented using the simplified scheme explained earlier in this chapter. The strains induced in the cohesive layers are calculated using FEA and are used to quantify TPB zone damage using a strain-based criterion, that is, separation in the cohesive layers, as explained later.

4.4 Results and discussion

Cohesive elements give rise to numerical convergence and stability issues that are well documented in the literature. Unstable behavior of cohesive elements due to negative stiffness (i.e., softening) in the damage evolution phase causes local instability in the electrode models used in this study. The local stabilization algorithm available in Abaqus is used along with viscous regularization for the cohesive elements to address convergence and stability issues. Small values of the viscosity parameter (μ = 0.001–0.01) are used to ensure that the energy quantities dissipated in regularization and stabilization are small compared with the strain energy in the model. Fixed boundary conditions (BCs) are prescribed by fixing all degrees of freedom (DOFs) at each node on each face of the models. The 3-D cathode model with cohesive zones is subjected to steady-state temperature change from room temperature (20°C) up to operating temperature. Spatially uniform temperature fields of increasing magnitude (120°C, 220°C,..., 820°C) are used to apply increasing levels of thermal loads (ΔT = 100°C, 200°C,..., 800°C). Similar analyses are performed for the 3-D cathode model without cohesive zones. Energy quantities (e.g., strain energy and damage dissipation) are computed from each FE analysis. **Figure 6** also shows the interface zones between dissimilar solid phases that are composed of cohesive elements.

Figure 7 shows energy quantities obtained from the FE analyses of cathode models with and without cohesive interface zones. The energy quantities are plotted as functions of temperature, which show a comparison between the strain energies of the cohesive model and the non-cohesive model. The energy dissipated due to damage (i.e., the damage dissipation) in the interface zones of the cohesive cathode model is plotted as a function of temperature in **Figure 8**. It is observed from **Figure 7** that the strain energy of the cohesive and non-cohesive cathode models increases with increasing temperature, as expected from the larger thermal stresses induced at higher temperatures, with fixed boundary conditions.

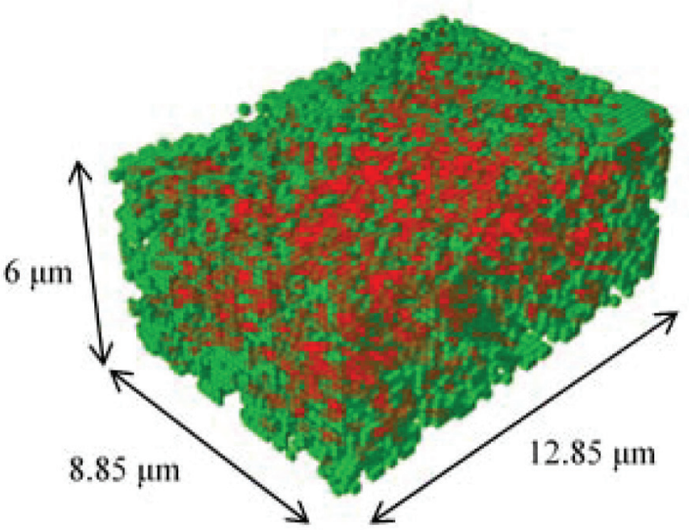

Figure 6.
Cathode model with horizontal interface zones.

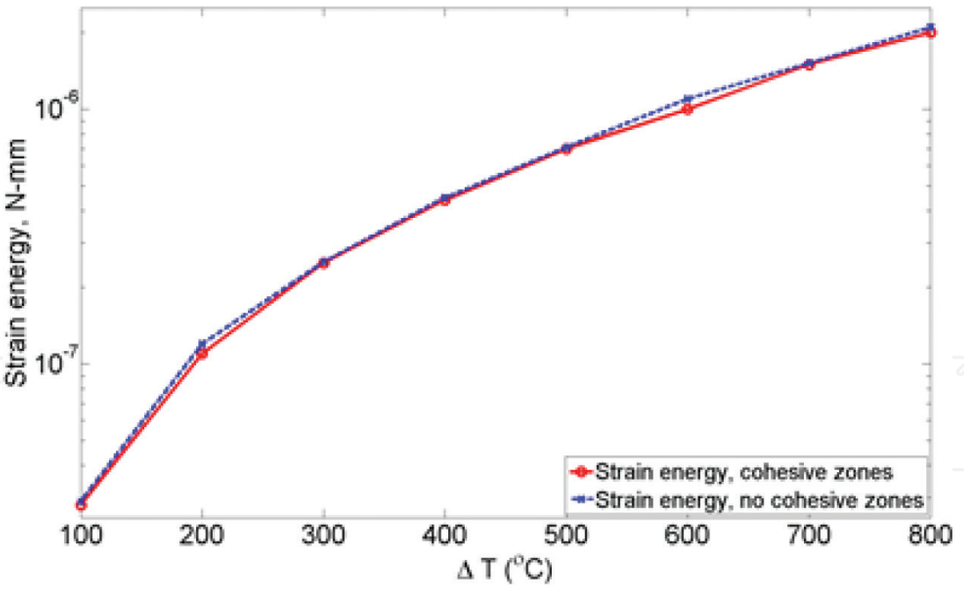

Figure 7.
Strain energy in cathode models with and without cohesive interface zones.

Similarly, from **Figure 8**, it is seen that the energy dissipated due to interfacial damage in the cohesive model also increases with increasing temperature, since more damage occurs at higher temperatures. A significant feature of **Figure 7** is that the strain energy of the non-cohesive model is slightly higher than that of the cohesive model at all temperatures. The physical explanation of the earlier observations is as follows. From the first law of thermodynamics and the Griffith energy balance statement for fracture (i.e., damage), we know that a damage process (e.g., cracking) can occur in a system only if this process causes the total energy of the system to either decrease or remain constant. The limiting condition is attained when damage occurs at equilibrium conditions, with the total energy remaining constant [30]:

$$\frac{dE}{dA} = \frac{d\Pi}{dA} + \frac{dW_s}{dA} = 0 \tag{5}$$

where E is the total energy of the system, Π is the potential energy of the system = U–F, U is the strain energy of the system, F is the work done by external

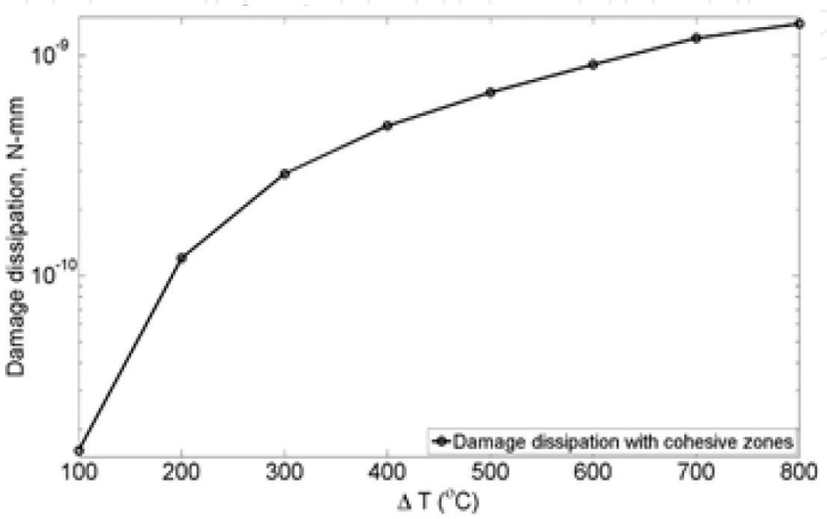

Figure 8.
Damage dissipation in cathode model with cohesive zones.

forces, W_s is the work required for creating new surfaces, and A is the damage variable (e.g., crack length).

In the cathode models analyzed, fixed boundary conditions are prescribed. This means that all translational and rotational DOFs at each node on each face of the model are set to zero. Thus, this model can be regarded as a displacement controlled model [30], with the displacement of the faces fixed at zero. For a displacement controlled system, we know that the external work is zero (F = 0). This is confirmed by the numerical values of the external work obtained from FEA, which are on the order of 10^{-40}. Thus, for a displacement controlled system, Π = U. Finally, from Irwin's energy release rate analysis [30], we know that for displacement control the strain energy of the system decreases as damage (e.g., cracking) occurs. This explains the lower strain energy of the cohesive model as compared to the non-cohesive model at a given temperature.

The second objective of this study is to approximately simulate the effects of thermal cycling on electrode integrity and performance using monotonic, steady-state, thermal loads coupled with an interface strength degradation scheme. In order to achieve this, the electrode models (cathode: 50:50 wt.% LSM:YSZ) with cohesive zones are subjected to five successive analyses. Each analysis represents the heating phase of a normalized thermal cycle, with one normalized cycle being taken equal to 1000 cycles. Only the heating phase of the thermal cycle is simulated in each analysis. Steady-state conditions are assumed and transient effects are neglected. Starting from a uniform initial room temperature of 20°C, the models are subjected to steady-state temperature change up to an operating temperature of 820°C using a spatially uniform temperature field. During each successive analysis, progressive interface degradation is simulated by decreasing the interface strength and fracture energy of the cohesive layers. Two separate interface strength degradation schemes are studied. In the first scheme (Scheme 1), the initial interface strength is assumed to decrease by 5 MPa in each successive cycle. In the second scheme (Scheme 2), the interface strength is assumed to decrease by 10 MPa in each successive cycle. The constitutive thickness of each cohesive element is set equal to 1.0, so that the nominal strain components (ε) calculated using FE analysis are numerically equal to the respective separation components (δ).

Figure 9 shows the interface strength reduction schemes employed to study TPB evolution in the cathode under repeated thermal loading, that is, Scheme 1 (Δt_i^0 = - 5 MPa per cycle, where t_i^0 = interface strength) and Scheme 2 (Δt_i^0 = - 10 MPa per cycle).

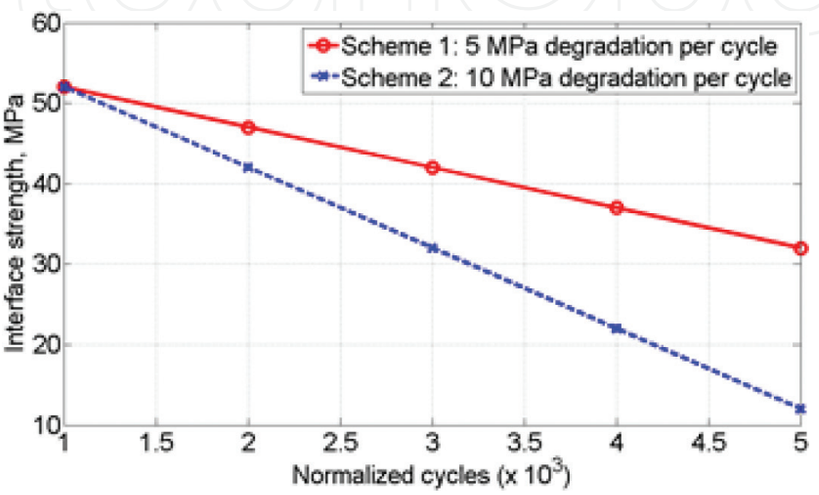

Figure 9.
Interface strength evolution schemes: LSM/YSZ interface.

The numerical values of interface strength and fracture energy used in Scheme 1 (Δt_i^0 = - 5 MPa per cycle) and Scheme 2 (Δt_i^0 = - 10 MPa per cycle) are given in **Table 2**.

Pitakthapanaphong and Busso [11] have performed numerical simulations to determine the critical energy release rates (G_i) for several material interfaces encountered in SOFC systems. Numerically, these values vary from 7.80 J m^{-2} for LSM/YSZ interface to 38.70 J m^{-2} for LSM-LSCoO interface. From these data, it can be concluded that the interface fracture energy values used in this study (**Table 2**) are physically reasonable. Cathode models with fixed boundary conditions (BCs) are used in this study.

The models are subjected to repeated, monotonic, steady-state heating as explained earlier, and the thermal stresses and strains are calculated through FEA. The strains induced in each cohesive element are written to the output data file associated with each analysis, along with strain energy and damage dissipation values. The strains are used to calculate the evolution of three-phase boundaries (TPBs) with thermal cycling, as explained in the next subsection. The energy quantities are used to study the mechanical degradation of the overall model. The TPB length at each temperature is calculated as follows. First, an electrode model without cohesive zones is created by image stacking (using a cell array data structure in MATLAB). The original 2-D images used to reconstruct the 3-D microstructure are stored as pixel value arrays in the cell array. In each 2-D image, boundary pixels are identified by pixel value comparison of each pixel with its eight adjacent in-plane neighbors. Boundary pixels are stored as black pixels (pixel value = 0) at corresponding locations in an initially empty "boundary point" cell array of identical size as the image cell array. Interior (i.e., non-boundary) locations are stored as white pixels at corresponding locations in the boundary point cell array. Using the boundary point cell array, locations of boundary pixels in the image array are identified as black pixels in the boundary point array, and the pixel value of the boundary pixel at the corresponding location in the image array is checked. The pixel values of the eight pixels adjacent to that boundary pixel are also checked to test whether all three phases are present at that boundary location. If so, the location is stored as a three-phase boundary (TPB) point (black pixel) in another initially empty "TPB" cell array. All other non-TPB locations are stored as white pixels in the TPB array. After TPB locations have been identified, the total number of TPB points is counted, and multiplied by the z-distance between images, to obtain the total undamaged TPB length (μm) in the electrode models. The total undamaged TPB length (μm) is divided by the volume (μm^3) of the 3-D electrode model to obtain the TPB density (μm^{-2}) in the model. Damage accumulation over five normalized cycles is calculated by determining the failed TPB cohesive elements in each cycle that had not failed in the previous cycle. The difference between the number of failed TPB elements in the (n + 1)th cycle and in the nth cycle is used to quantify the additional TPB loss in each

Normalized cycles (x 10^3)	**Interface strength, MPa (Scheme 1)**	**Interface strength, MPa (Scheme 2)**	**Interface fracture energy, J m^{-2} (Scheme 1)**	**Interface fracture energy, J m^{-2} (Scheme 2)**
1	52	52	7.80	7.80
2	47	42	7.05	6.30
3	42	32	6.30	4.80
4	37	22	5.55	3.30
5	32	12	4.80	1.80

Table 2.
Cathode model: interface strength and fracture energy data.

successive cycle, and the cumulative TPB loss over N such cycles is thus determined by successively adding the new damage in each cycle to the cumulative total damage over the previous (N - 1) cycles. The model used in this study for evaluating cumulative TPB damage with thermal cycling may be regarded as a simple model for calculating cumulative fatigue damage. A detailed mathematical model for predicting the lifetime of planar SOFCs subjected to thermal cycling has been developed by Liu et al. [31]. That model uses Paris' law and cracks nucleation concepts to derive expressions for damage distribution in the interfacial layers of planar SOFCs under thermal cycling. It predicts that the number of cycles required for failure will decrease with increase in electrolyte thickness and electrode porosity [31].

Figure 10 depicts the change in the strain energy content of the cathode with thermal cycling. **Figure 10** shows that for both interface degradation schemes, the strain energy of the model progressively decreases over five normalized thermal cycles. This is expected from the progressive mechanical degradation of the interfaces within the model with thermal cycling.

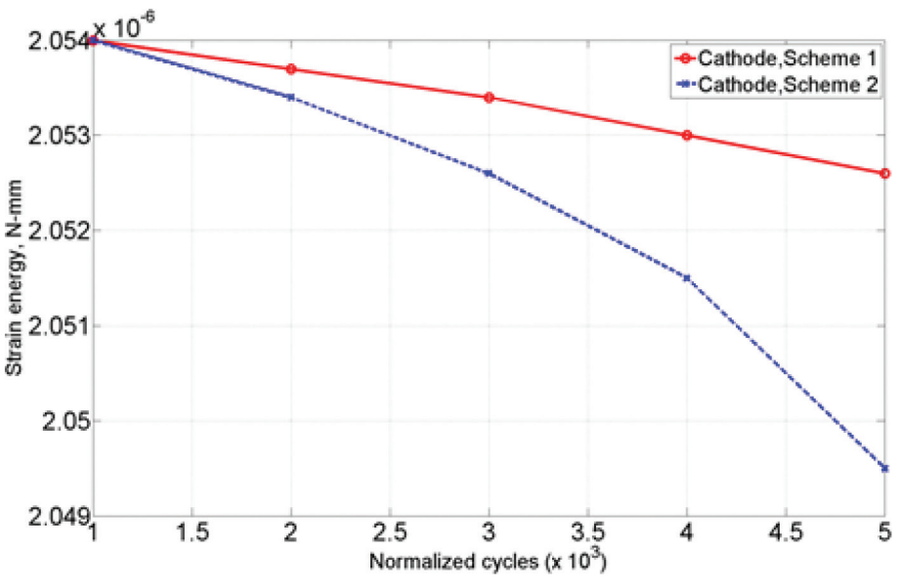

Figure 10.
Strain energy evolution for cathode model with thermal cycling.

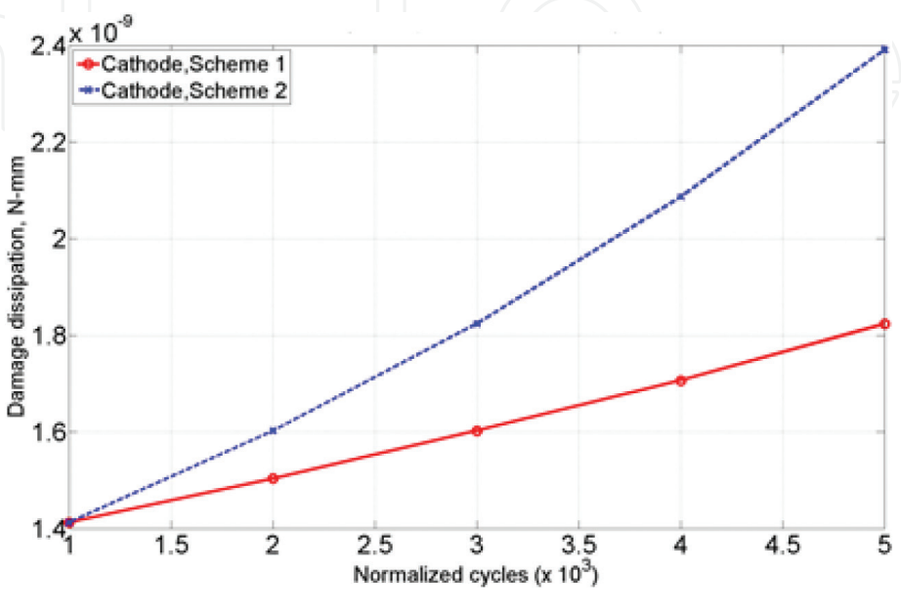

Figure 11.
Damage dissipation in cathode model with thermal cycling.

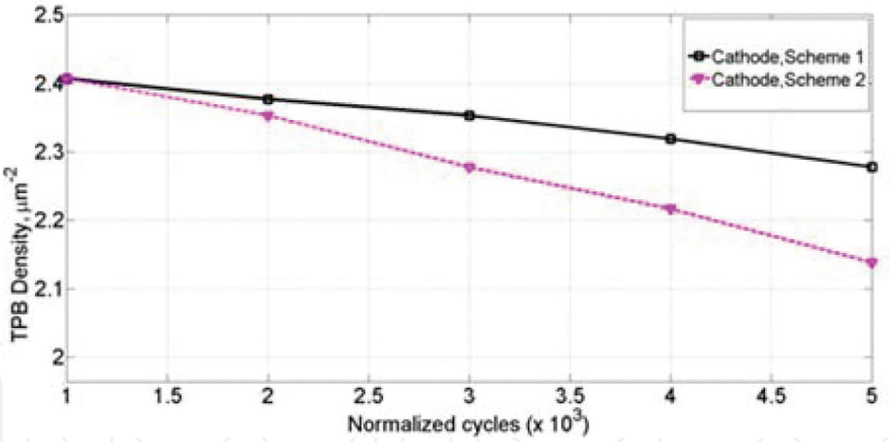

Figure 12.
TPB density evolution with thermal cycling for electrode models.

Such progressive interface degradation leads to a cumulative dissipation of energy due to damage and hence to a progressive decrease in strain energy content of the model. This is further illustrated in **Figure 11**, which shows the cumulative damage dissipation with thermal cycling. As expected, Scheme 2 ($\Delta\, t_i^0 = -10$ MPa per cycle) leads to lower strain energy content, and larger cumulative damage dissipation, than Scheme 1 ($\Delta\, t_i^0 = -5$ MPa per cycle).

Figure 12 shows the evolution of the TPB density with thermal cycling for the anode and cathode models considered in this study. **Figure 12** simultaneously compares the TPB density evolution for cathode versus anode and for Scheme 1 ($\Delta t_i^0 = -5$ MPa per cycle) versus Scheme 2 ($\Delta t_i^0 = -10$ MPa per cycle).

The TPB density of cathode model decreases over the five successive normalized thermal cycles ($\Delta T = +800°C$), as expected from the progressive degradation of the interface with thermal cycling. As expected for the cathode model, Scheme 2 (10 MPa degradation per cycle) leads to a lower final TPB density than Scheme 1 (5 MPa degradation per cycle), after five normalized heating cycles. The TPB density of the cathode undergoes a large reduction (5.36% for Schemes 1, 11.18% for Scheme 2). Wilson et al. [10] have cited TPB density values lying in the range of 1.7–6.5 μm^{-2} for cathodes and have reported cathode TPB density values in the range 6–9 μm^{-2} [12]. From these experimental data, it may be concluded that the TPB density values obtained in this study for the cathode (2.138–2.407 μm^{-2}) are physically reasonable.

5. Conclusion

2-D images of solid oxide fuel cell (SOFC) cathode microstructures (50:50 wt.% LSM:YSZ) are used to perform 3-D finite element models. The effect of LSM/YSZ interface degradation under repeated thermal loading on mechanical integrity and electrochemical performance of SOFC electrodes is simulated by implementing a simplified damage scheme in cathode FE models with cohesive interface zones. The cathode model is first subjected to increasing levels of thermal load using spatially uniform temperature fields. Energy quantities for models with and without cohesive interface zones are obtained through FEA. These quantities are compared using energy balance concepts from fracture mechanics to gain insight into the effects of interface degradation on mechanical integrity. The effect of interface degradation with increasing temperature on the mechanical integrity of a displacement controlled cathode microstructure model is clearly seen as a reduction in strain energy

of the model due to damage dissipation. The evolution of three-phase boundary (TPB) zones in electrode microstructure models with thermal cycling [32] is studied by implementing an interface damage scheme that includes reduction of both interface strength and fracture energy. It is found that TPB density decreases over a number of normalized heating cycles. Degradation of the mechanical integrity of the cathode model under repeated thermal loading is also observed, in the form of progressively decreasing strain energy content due to cumulative damage dissipation with thermal cycling. These observations indicate that interface damage may be a major mechanism responsible for SOFC performance degradation over time.

Acknowledgements

The financial support for this work from the National Science Foundation under the Faculty Early Career Development (CAREER) Grant CMMI-0546225 (Material Design & Surface Engineering Program) is gratefully acknowledged.

Conflict of interest

There is no conflict of interest.

Author details

Sushrut Vaidya[1] and Jeong ho Kim[2*]

1 Department of Civil Engineering, Mahindra Ecole Centrale, Hyderabad, Telangana, India

2 Department of Civil and Environmental Engineering, University of Connecticut, Storrs, CT, USA

*Address all correspondence to: jeongho.kim@uconn.edu

References

[1] Singhal SC, Kendall K, editors. High Temperature Solid Oxide Fuel Cells: Fundamentals, Design and Applications. Oxford: Elsevier Ltd.; 2003

[2] Laurencin J, Delette G, Lefebvre-Joud F, Dupeux M. A numerical tool to estimate SOFC mechanical degradation: Case of the planar cell configuration. Journal of the European Ceramic Society. 2008;**28**:1857-1869

[3] Zhang T, Zhu Q, Huang WL, Xie Z, Xin X. Stress field and failure probability analysis for the single cell of planar solid oxide fuel cells. Journal of Power Sources. 2008;**182**:540-545

[4] Giraud S, Canel J. Young's modulus of some SOFCs materials as a function of temperature. Journal of the European Ceramic Society. 2008;**28**:77-83

[5] Selcuk A, Atkinson A. Strength and toughness of tape-cast yttria-stabilized zirconia. Journal of the American Ceramic Society. 2000;**83**(8):2029-2035

[6] Toftegaard H, Sorensen BF, Linderoth S, Lundberg M, Feih S. Effects of heat-treatments on the mechanical strength of coated YSZ: An experimental assessment. Journal of the American Ceramic Society. 2009;**92**(11):2704-2712

[7] Selcuk A, Atkinson A. Elastic properties of ceramic oxides used in solid oxide fuel cells (SOFC). Journal of the European Ceramic Society. 1997;**17**:1523-1532

[8] Pihlatie M, Kaiser A, Mogensen M. Mechanical properties of NiO/Ni-YSZ composites depending on temperature, porosity and redox cycling. Journal of the European Ceramic Society. 2009;**29**:1657-1664

[9] Wilson JR, Kobsiriphat W, Mendoza R, Chen H-Y, Hiller JM, Miller DJ, Thornton K, Voorhees PW, Adler SB, Barnett SA. Three-dimensional reconstruction of a solid-oxide fuel-cell anode. Nature Materials. 2006;**5**:541-544

[10] Wilson JR, Duong AT, Gameiro M, Chen H-Y, Thornton K, Mumm DR, Barnett SA. Quantitative three-dimensional microstructure of a solid oxide fuel cell cathode. Electrochemistry Communications. 2009;**11**:1052-1056

[11] Wilson JR, Barnett SA. Solid oxide fuel cell Ni-YSZ anodes: Effect of composition on microstructure and performance. Electrochemical and Solid-State Letters. 2008;**11**(10):B181-B185

[12] Wilson JR, Cronin JS, Duong AT, Rukes S, Chen H-Y, Thornton K, Mumm DR, Barnett S. Effect of composition of ($La_{0.8}Sr_{0.2}MnO_3$-Y_2O_3-stabilized ZrO_2) cathodes: Correlating three-dimensional microstructure and polarization resistance. Journal of Power Sources. 2010;**195**:1829-1840

[13] Goldin GM, Zhu H, Kee RJ, Bierschenk D, Barnett SA. Multidimensional flow, thermal, and chemical behavior in solid-oxide fuel cell button cells. Journal of Power Sources. 2009;**187**:123-135

[14] Selimovic A, Kemm M, Torisson T, Assadi M. Steady state and transient thermal stress analysis in planar solid oxide fuel cells. Journal of Power Sources. 2005;**145**:463-469

[15] Anandakumar G, Li N, Verma A, Singh P, Kim J-H. Thermal stress and probability of failure analyses of functionally graded solid oxide fuel cells. Journal of Power Sources. 2010;**195**:6659-6670

[16] Clague R, Shearing PR, Lee PD, Zhang Z, Brett DJL, Marquis AJ, Brandon NP. Stress analysis of solid oxide fuel cell anode microstructure reconstructed from focused ion beam tomography. Journal of Power Sources. 2011;**196**:9018-9021

[17] Vaidya S, Kim J-H. Continuum mechanics of solid oxide fuel cells using three-dimensional reconstructed microstructures. In: Gan YX, editor. Continuum Mechanics – Progress in Fundamentals and Engineering Applications. Rijeka: InTech; 2012. pp. 73-88

[18] Zhu W, Ding D, Xia C. Enhancement in three-phase boundary of SOFC electrodes by an ion impregnation method: A modeling comparison. Electrochemical and Solid-State Letters. 2008;**11**:B83-B86

[19] Abaqus v6.11, Dassault Systemes Simulia Corp., Providence, Rhode Island

[20] MATLAB ®R2010a, the MathWorks, Inc., Natick, Massachusetts

[21] Vivet N, Chupin S, Estrade E, Richard A, Bonnamy S, Rochais D, Bruneton E. Effect of Ni content in SOFC Ni-YSZ cermets: A three-dimensional study by FIB-SEM tomography. Journal of Power Sources. 2011;**196**:9989-9997

[22] Johnson J, Qu J. Effective modulus and coefficient of thermal expansion of Ni-YSZ porous cermets. Journal of Power Sources. 2008;**181**:85-92

[23] Xiao J, Schneider H, Dönnecke C, König G. Wedge splitting test on fracture behaviour of ultra high strength concrete. Construction and Building Materials. 2004;**18**:359-365

[24] Nguyen BN, Koeppel BJ, Ahzi S, Khaleel MA, Singh P. Crack growth in solid oxide fuel cell materials: From discrete to continuum damage modeling. Journal of the American Ceramic Society. 2006;**89**:1358-1368

[25] Kakac S, Pramuanjaroenkij A, Zhou XY. A review of numerical modeling of solid oxide fuel cells. International Journal of Hydrogen Energy. 2007;**32**:761-786

[26] Atkinson A, Selçuk A. Mechanical behavior of ceramic oxygen ion-conducting membranes. Solid State Ionics. 2000;**134**:59-66

[27] Ebrahimi F, Bourne G, Kelly MS, Matthews T. Mechanical properties of nanocrystalline nickel produced by electrodeposition. Nanostructured Materials. 1999;**11**:343-350

[28] Janssen M, Zuidema J, Wanhill RJH. Fracture Mechanics. 2nd ed. VSSD. New York: Spon Press; 2006

[29] Meyers M, Chawla K. Mechanical Behavior of Materials. Upper Saddle River, New Jersey, New York: Prentice Hall, Cambridge University Press; 1999

[30] Anderson TL. Fracture Mechanics: Fundamentals and Applications. 4th ed. CRC press; 2005

[31] Liu L, Kim G-Y, Chandra A. Modeling of thermal stresses and lifetime prediction of planar solid oxide fuel cell under thermal cycling conditions. Journal of Power Sources. 2010;**195**:2310-2318

[32] Vaidya S, Kim J-H. Finite element thermal stress analysis of solid oxide fuel cell cathode microstructures. Journal of Power Sources. 2013;**225**:269-276

IntechOpen